ACS NANO

www.acsnano.org

ARTICLE

Dendron–Polymer Hybrids as Tailorable Responsive Coronae of Single-Walled Carbon Nanotubes

Verena Wulf, Gadi Slor, Parul Rathee, Roey J. Amir,* and Gili Bisker*

Cite This: *ACS Nano* 2021, 15, 20539–20549

Read Online

ACCESS | Metrics & More | Article Recommendations | Supporting Information

ABSTRACT: **Functional composite materials that can change their spectral properties in response to external stimuli have a plethora of applications in fields ranging from sensors to biomedical imaging. One of the most promising types of materials used to design spectrally active composites are fluorescent single-walled carbon nanotubes (SWCNTs), noncovalently functionalized by synthetic amphiphilic polymers. These coated SWCNTs can exhibit modulations in their fluorescence spectra in response to interactions with target analytes. Hence, identifying new amphiphiles with interchangeable building blocks that can form individual coronae around the SWCNTs and can be tailored for a specific application is of great interest. This study presents highly modular amphiphilic polymer-dendron hybrids, composed of hydrophobic dendrons and hydrophilic polyethylene glycol (PEG) that can be synthesized with a high degree of structural freedom, for suspending SWCNTs in aqueous solution. Taking advantage of the high molecular precision of these PEG-dendrons, we show that precise differences in the chemical structure of the hydrophobic end groups of the dendrons can be used to control the interactions of the amphiphiles with the SWCNT surface. These interactions can be directly related to differences in the intrinsic near-infrared fluorescence emission of the various chiralities in a SWCNT sample. Utilizing the susceptibility of the PEG-dendrons toward enzymatic degradation, we demonstrate the ability to monitor enzymatic activity through changes in the SWCNT fluorescent signal. These findings pave the way for a rational design of functional SWCNTs, which can be used for optical sensing of enzymatic activity in the near-infrared spectral range.**

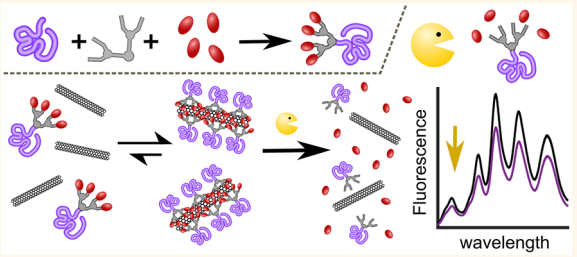

KEYWORDS: *single-walled carbon nanotubes, optical nanosensors, fluorescent nanoparticles, dendritic amphiphiles, enzyme-responsive materials*

Single-walled carbon nanotubes (SWCNTs) find broad applications as biomedical sensors, mainly due to their intrinsic fluorescence emission in the near-infrared (NIR) transparency window of biological tissue, that allow for *in vitro* and *in vivo* sensing also in deeper tissue.[1−7] SWCNTs can be described as graphene sheets rolled up into cylinders, resulting in nanotubes with different (n,m)-chiralities, depending on their roll-up vector.[8] The fluorescence emission peak intensities and wavelengths of a SWCNT-sample are dependent on its composition of nanotubes with different chiralities and the dielectric environment and are usually between 900 and 1500 nm.[9−11]

Owing to their graphene-like surface, SWCNTs are highly hydrophobic nanostructures that require functionalization with dispersants such as low molecular weight surfactants,[12] single-stranded DNA,[13] RNA,[14] suitable proteins,[15,16] peptides,[17,18] peptoids,[19] or amphiphilic polymers,[20,21] in order to form colloidal suspensions in aqueous media. The interactions enabling a dispersant to bind the SWCNT surface are primarily $\pi-\pi$ stacking between the graphene lattice and aromatic groups (DNA, polymers)[13] or hydrophobic interactions (surfactants, phospholipids).[15]

For sensing applications, the dispersing agents require either to contain a recognition element specific for the desired analyte (*e.g.*, aptamers, antibodies, binding peptides)[2,22−24] or to wrap the SWCNTs forming a so-called corona phase that, due to its structure, conformation, and charge is able to selectively bind certain analytes.[19,25−28] The dispersants forming the latter group are very often amphiphilic polymers that do not suffer from effects like aging or biodegradation

Received: October 15, 2021
Accepted: December 2, 2021
Published: December 8, 2021

https://doi.org/10.1021/acsnano.1c09125
ACS Nano 2021, 15, 20539–20549

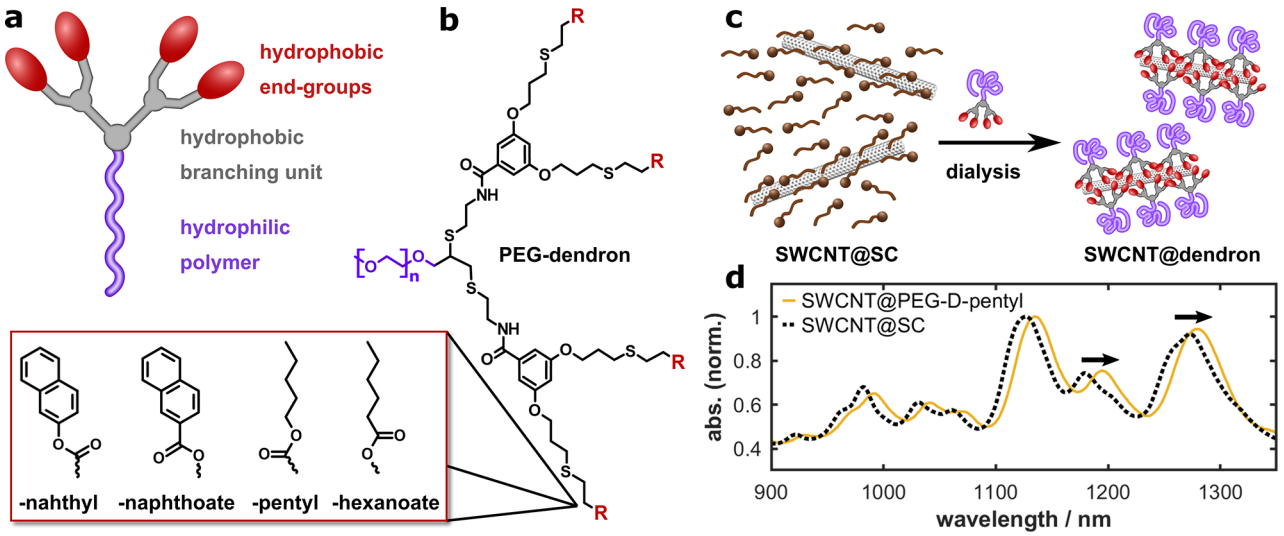

Figure 1. Polymer-dendron hybrids are modular amphiphilic macromolecules capable to disperse SWCNTs. (a) Schematic representation and chemical structure of the amphiphilic polymer-dendron hybrids consisting of a hydrophilic polymer chain (purple) and a hydrophobic dendron (gray) that bears hydrophobic end groups (red). (b) Polyethylene glycol (PEG, 5 kDa) serves as the hydrophilic chain, coupled to a dendron branching into four identical hydrophobic end groups. The hydrophobic end groups, naphthyl, naphthoate, pentyl, and hexanoate, differ in their aromaticity (naphthalene-based or aliphatic) and in the orientation of an ester group. (c) Functionalization of SWCNTs with the polymer-dendron amphiphiles (SWCNT@PEG-dendrons) was performed *via* surfactant exchange from sodium cholate suspended SWCNTs (SWCNT@SC). SWCNT@SC together with PEG-dendrons are dialyzed against water to slowly remove sodium cholate and enable attaching of the PEG-dendrons. (d) Absorption spectra of the SWCNT@PEG-dendrons, here shown for SWCNT@PEG-D-pentyl (yellow solid line), compared to the initial absorption of SWCNT@SC (black dashed line), show a red shift consistent with a change in the dielectric environment of the SWCNTs, due to the binding of the PEG-dendron amphiphiles.

compared to aptamers or binding proteins. Upon the interaction with the target analyte, the emitted fluorescence of the SWCNTs is modulated. Corona-based recognition was reported for different types of analytes, including small biomolecules,[25,26,29] and even proteins.[27,28,30−34] The importance of the nature of the exposed, hydrophilic part of the amphiphilic dispersant in forming an analyte-specific corona phase is evident, but previous publications reveal that the corona phase is also influenced by its hydrophobic anchor unit, attached to the SWCNTs. For the recognition of fibrinogen, SWCNTs suspended by a polyethylene glycol (PEG) polymer coupled to a phospholipid with a chain length of 16 carbon atoms were found to have the highest optical response, while coupling to a phospholipid with 14 or 18 carbon atoms showed significantly weaker response.[27] This hints to the fact that the polymer, which is exposed to the solution and thus to the analyte, as well as the hydrophobic anchor of the amphiphile both play equally important roles in the formation of the corona phase.

Recently, several approaches have emerged for producing libraries of amphiphilic linear copolymers and block copolymers that can be used for suspending SWCNT for specific applications.[35] These include combinatorial high-throughput screening of a library of polymers,[25−27] high-throughput directed evolution,[36,37] reversible addition−fragmentation chain transfer polymerization,[38,39] and random peptide synthesis.[40,41] Nevertheless, challenges such as elaborated synthesis, multiple processing steps, or limited control over the final product, give rise to the need for different approaches for generating a library of highly versatile amphiphilic polymers with a wide range of molecular structures and functions. The future of corona phase sensing applications is thus dependent on the development of additional possibilities to create libraries of amphiphilic molecules.

Dendrons are tree-like molecular structures with multiple end groups, depending on the number of branching points, *i.e.*, the dendron generation, and a focal point that enables coupling, *e.g.*, to a polymer. Dendrons can vary in flexibility, size, and hydrophobicity, providing high degrees of freedom and molecular precision in creating hydrophobic structures. Combining hydrophobic dendrons bearing hydrophobic end groups with hydrophilic polymers, yields amphiphilic polymer-dendron hybrids.[42−44] The stability of micellar assemblies of these amphiphilic macromolecules, in particular PEG-dendron hybrids, have been widely studied and found to be dependent on the amphiphilic ratio between the polymer tail and the hydrophobic dendron.[44,45] Dendrons can be coupled to a variety of polymers to create a library of amphiphilic molecules with the ability to suspend SWCNTs in aqueous environment and providing designable wrapping agents to address the requirements of a particular application.[46] Previously, polystyrene coupled to pyrene-functionalized dendrons were reported to suspend SWCNTs in THF,[47] while hydrophilic dendrons coupled to a hydrophobic alkyl-chain or pyrene have been reported to suspend SWCNTs in water, due to increasing hydrophilicity with increasing dendron generation.[48−51] Nevertheless, designing hydrophobic dendrons as the binding sites provides a high degree of control over tuning their direct interaction with the SWCNT surface.[52]

In this study, we present polymer-dendron hybrids as modular amphiphilic agents for the suspension of SWCNTs in aqueous media. The polymer-dendron hybrids designed for this study are amphiphilic macromolecules consisting of three structural elements (Figure 1a): (I) a linear polymer chain serving as the hydrophilic block, whose hydrophilicity and flexibility depends on its chemical composition and its length, (II) the dendron body acting as part of the hydrophobic block, whose size, flexibility, and hydrophobicity are determined by

https://doi.org/10.1021/acsnano.1c09125
ACS Nano 2021, 15, 20539−20549

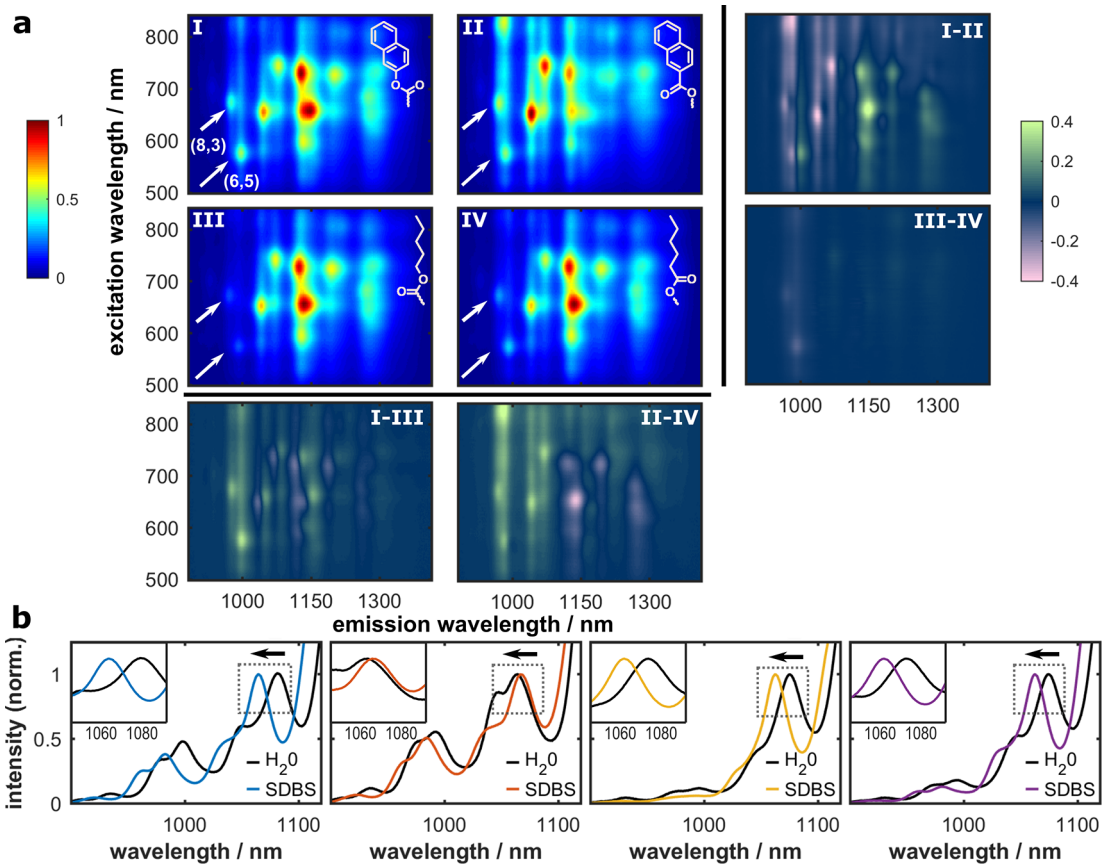

Figure 2. Fluorescence emission of SWCNT@PEG-dendrons reveal chirality-dependent fluorescence emission for the different end groups. (a) Normalized fluorescence excitation−emission spectra for SWCNT@PEG-D-naphthyl (I), SWCNT@PEG-D-naphthoate (II), SWCNT@PEG-D-pentyl (III), and SWCNT@PEG-D-hexanoate (IV), each at a SWCNT concentration of 5 mg L^{-1}. Differences between the two SWCNT@PEG-dendron samples with aromatic polymer-dendrons (I−II) and differences between the two SWCNT@PEG-dendron samples with aliphatic polymer-dendrons (III−IV). Differences between the two SWCNT@PEG-dendron samples with their ester group in the same orientation (I−III) and (II−IV). Arrows mark the fluorescence emission of the (6,5) and the (8,3) chiralities. (b) Normalized fluorescence emission before (black) and after the addition of 0.2% (w/v) SDBS to a 1 mg L^{-1} suspensions of SWCNT@PEG-D-naphthyl (blue), SWCNT@PEG-D-naphthoate (red), SWCNT@PEG-D-pentyl (yellow), SWCNT@PEG-D-hexanoate (purple). Insets: wavelength shift ($\Delta\lambda$) of the (10,2) chiralities are calculated to be $\Delta\lambda$ = −16.7 nm, 4.1 nm, −12.6 nm, and −11.9 nm (from left to right).

the chemical structure of the branching units and the dendron's generation, and (III) a number of hydrophobic end groups that are covalently attached to the dendron and whose number depends on the generation of the dendron. The key benefits of using dendrons as the hydrophobic block that is interacting with the SWCNTs in comparison with linear architectures are the structural symmetry of the dendritic end groups as well as their high spatial availability to interact with the surface of the SWCNTs, due to being presented at the termini of the dendritic branches. To shed light on the effect of the dendritic end groups on the corona phase around the SWCNTs, and the resulting optical properties, we designed PEG-dendron amphiphiles with end groups that can differ in their interactions with the carbon nanotube surface. Taking advantage of the high modularity and simplicity of the synthetic pathway, we studied the influence of precise changes in the chemical structure of the end groups on the fluorescence emission of the SWCNTs. To further understand and exploit the nature of the specific interactions between the anchoring end groups and the SWCNTs surface, we utilized the ester bonds between the hydrophobic end groups and the dendron to study the response of the SWCNTs to esterase as a model enzyme. We tested the reactivity of the PEG-dendrons corona of the SWCNTs toward enzymatic activity *via* fluorescence spectroscopy in the NIR spectral region. Building on these results, we further designed a SWCNT@PEG-dendron composite for monitoring enzymatic amide cleavage, demonstrating the generality of this sensing platform.

RESULTS AND DISCUSSION

The dendron−polymer hybrids, applied in this study, contain monomethoxy polyethylene glycol as the hydrophilic polymer chain. PEG was proven to be a suitable polymer for the dispersion of SWCNTs, providing a hydrophilic shell for their stable suspensions in water and biological media and being relatively inert toward protein interaction.[27,32,53] The dendritic architecture exposes four hydrophobic end groups, enabling noncovalent binding to the SWCNTs. To create a set of polymer-dendrons, two aliphatic and two aromatic (naphthalene-based) end groups were coupled *via* an ester group in two different orientations to the dendritic body (Figure 1b), resulting in PEG-D-naphthyl, PEG-D-naphthoate, PEG-D-pentyl, and PEG-D-hexanoate. The orientation of the ester group in the end groups places either an electron donor (alkoxy group of the ester) for PEG-D-naphthyl or an electron acceptor (carbonyl group of the ester) for PEG-D-naphthoate

https://doi.org/10.1021/acsnano.1c09125
ACS Nano 2021, 15, 20539−20549

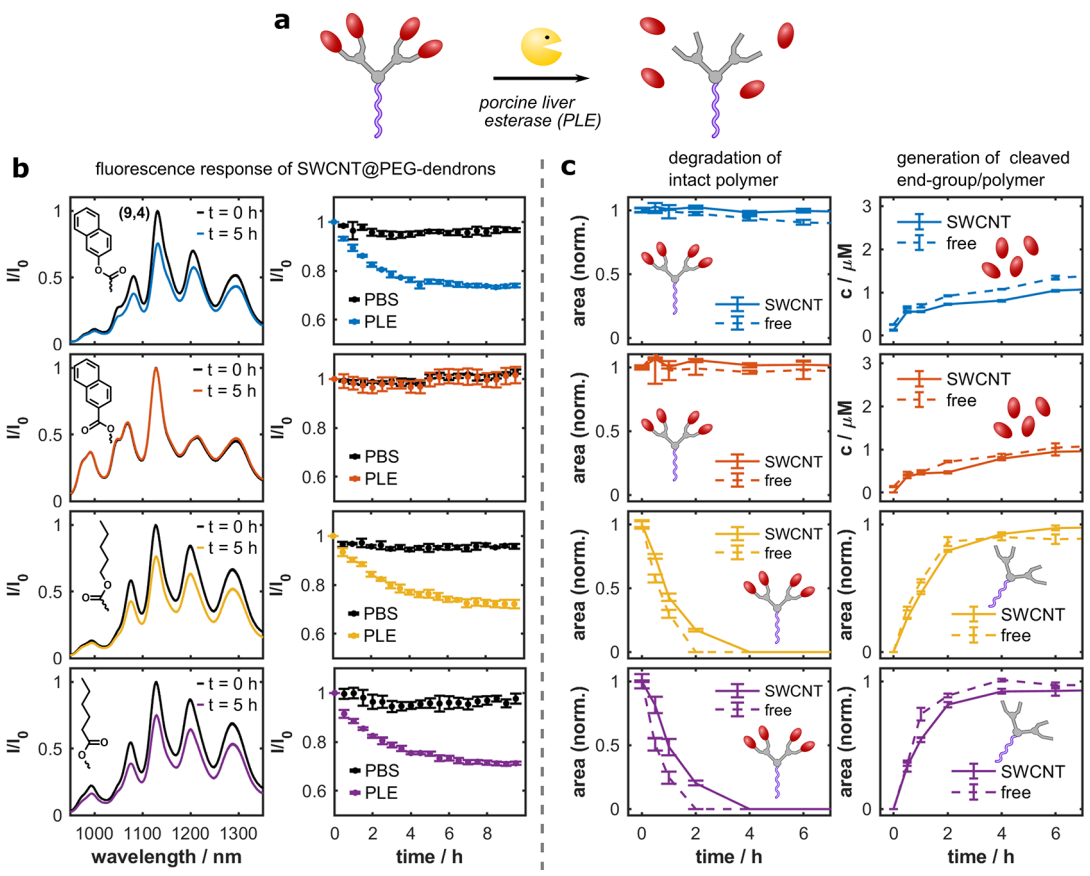

Figure 3. Enzymatic cleavage of PEG-dendrons with porcine liver esterase (PLE). (a) Cleavage of the PEG-dendrons by PLE takes place at the ester group connecting the end groups to the dendron body. (b) Fluorescence response of SWCNT@PEG-D-naphthyl (blue), SWCNT@PEG-D-naphthoate (red), SWCNT@PEG-D-pentyl (yellow), and SWCNT@PEG-D-hexanoate (purple) each at a SWCNT-concentration of 1 mg L^{-1} upon incubation with PLE 1.5 μM for 5 h (λ_{ex} = 730 nm) and time-dependent fluorescence response after the addition of PLE of the peak intensity of the (9,4) chirality at λ_{ex} = 730 nm over 10 h compared to a sample in PBS (black dots). (c) Quantification of the degradation process of PEG-dendrons wrapping SWCNTs and as free micellar assemblies after separation *via* HPLC. Enzymatic degradation process at time intervals of 0, 0.5, 1, 2, 4, and 6 h. PEG-dendrons as free micellar assemblies in absence of SWCNTs (dashed lines) and as wrapping polymer around SWCNTs (solid lines). Left column: Degradation of the intact polymer, bearing all four end groups. Right column: Quantification of the concentration of the cleaved-off end groups naphthol (blue) and naphthoic acid (red). Generation of polymer-dendrons with cleaved-off end groups for PEG-D-pentyl (yellow) and PEG-D-hexanoate (purple).

in the vicinity of the delocalized π-electron system of the aromatic end group affecting its electron density. Due to their aromatic nature, these end groups should bind to the SWCNTs *via* $\pi-\pi$-stacking interactions, which are expected to be influenced by the electron density of the delocalized π-systems.[54] In contrast, the aliphatic end groups should interact with the SWCNTs *via* hydrophobic interactions. Hence, the orientation of the ester group is not expected to have an effect on the binding interaction. To avoid an effect due to changes in molecular weight, each couple of amphiphiles, was synthesized to have exactly the same molecular weight. This was achieved by reacting 3-mercaptopropionic acid with the 2-naphthol and pentanol for synthesizing the naphthyl and pentyl end groups, respectively, while using 2-mercaptoethanol for preparing the 2-naphthoate and hexanoate end groups (Scheme S3, Supporting Information).

Functionalization of the SWCNTs was achieved *via* surfactant exchange, where sodium cholate suspended SWCNTs (SWCNT@SC), together with the respective polymer-dendron, were dialyzed against water, to slowly remove sodium cholate allowing the PEG-dendrons to bind the SWCNTs and stabilize them in suspension (Figure 1c).[27] To ensure the critical role of the hydrophobic end groups in binding the SWCNTs, we performed the surfactant exchange also with a PEG-dendron bearing hydrophilic end groups as a control. This experiment resulted in SWCNT aggregation (Figure S1, Supporting Information), showing that the hydrophobic end groups are essential for stabilizing the suspended SWCNTs. The NIR-absorption spectra of the resulting PEG-dendron wrapped SWCNTs (SWCNT@PEG-dendron) showed a red shift of the E_{11}-absorption peaks (Figures 1d and S2, Supporting Information) as well as of the fluorescence emission of the SWCNT chiralities (Figure S3, Supporting Information) compared to SWCNT@SC, indicating a successful wrapping exchange consistent with a change in the dielectric environment of the SWCNTs.[55]

Each corona phase can influence the fluorescence emission of the SWCNTs, due to its density and/or interactions with the SWCNT surface. Fluorescence emission of a certain chirality can be altered by the distinct dielectric environment that the corona phase induces around the SWCNTs[56] or even charge transfer effects from the wrapping molecules to the SWCNT or vice versa.[57,58] Our PEG-dendrons are bound to the SWCNTs *via* end groups that differ in the type of their interaction with the graphene lattice. While $\pi-\pi$ stacking of the SWCNT with the aromatic end groups is possible,

https://doi.org/10.1021/acsnano.1c09125
ACS Nano 2021, 15, 20539−20549

hydrophobic interactions are expected in the case of the aliphatic end groups. Differences in these interactions are reflected in different fluorescence emission spectra of the SWCNT@PEG-dendron samples. While the four SWCNT@PEG-dendron show comparable absorption spectra of the E_{22} transitions (Figure S4, Supporting Information), we observed substantial differences in their fluorescence emission spectra of the E_{11} transitions, although all four samples were prepared from the same initial SWCNT@SC suspension. Figure 2a shows the NIR-fluorescence emission recorded for excitation wavelengths of λ_{ex} = 500−840 nm for the four different SWCNT@PEG-dendrons and the differences in the normalized fluorescence emission between the two PEG-dendrons with aromatic end groups and with aliphatic end groups, respectively. The orientation of the ester group in the case of the two PEG-dendrons with aromatic end groups, and the resulting difference of their electron density on $\pi-\pi$-stacking interactions had a substantial effect on SWCNT fluorescence modulation. The fluorescence intensity of SWCNT@PEG-D-naphthoate, which has electron withdrawing groups, is relatively lower, and the emission wavelength peaks of the different chiralities of the SWCNT@PEG-D-naphthyl, which has electron donating groups, are red-shifted, compared to the other SWCNT@PEG-dendrons, respectively (Figures 2a and S4, Supporting Information). However, for the two PEG-dendrons with aliphatic end groups, we observed comparable fluorescence emission, both in intensity and wavelength, since the orientation of the ester group has no effect on the hydrophobic interactions. Comparing the fluorescence spectra of the aromatic SWCNT@PEG-dendrons with their aliphatic counterparts, we observe substantially higher fluorescence emission of the small-diameter (8,3) and (6,5) chiralities (Figure 2a) for the aromatic amphiphiles. These variations cannot be attributed to simple differences in the concentration of the chiralities within the samples, as evident from the similar absorption spectra (Figure S4, Supporting Information), but rather to the distinct chemical properties of the end groups. The excitation−emission maps reveal the expected differences in the interaction of the dendritic end groups with the SWCNT surface.

The addition of surfactants, *e.g.*, sodium dodecylbenzenesulfonate (SDBS), to functionalized SWCNT can give information both about the available, exposed surface area of the SWCNTs, and the binding affinity of the dendrons to the SWCNTs by inducing a solvatochromic shift ($\Delta\lambda$) upon the replacement of water molecules and possibly some of the dendritic amphiphiles in case their binding affinity is lower than the binding affinity of the surfactant.[19,22,59−61] After the addition of 0.2% (w/v) SDBS to the different SWCNT@PEG-dendron samples, we see differences in the induced solvatochromic shifts, as shown in Figure 2b evaluated for the (10,2) chirality. While PEG-D-naphthoate shows the smallest wavelength shift of the (10,2) chirality of $\Delta\lambda$ = 4.1 nm, PEG-D-naphthyl shows the highest blue-shift caused by the addition of SDBS $\Delta\lambda$ = −16.7 nm. Both SWCNTs with aliphatic PEG-dendrons show comparable results with a blue shift of $\Delta\lambda$ = −12.6 nm and −11.9 nm, respectively. We can observe that SDBS is not able to completely replace the PEG-dendrons because of their higher affinity to the SWCNTs surface, as indicated by the fluorescence spectra of the different samples after the addition of SDBS, which still differ in their resonance wavelength and relative intensity (Figure 2b and S4).

After characterizing the spectral properties of the SWCNT@PEG-dendrons, we aimed to evaluate the ability to translate the enzymatic cleavage of the PEG-dendrons amphiphiles into a spectral response of the SWCNTs. The variations in the fluorescence modulation of the SWCNT@PEG-dendrons reveal not only different interactions between the PEG-dendrons and the SWCNT surface but also differences in their noncovalent binding stability. Amphiphilic PEG-dendrons are known to self-assemble into polymeric micelles, whose stability is dependent on their hydrophilic/hydrophobic ratio.[62−64] The ester group connecting the hydrophobic end groups to the dendritic branches is susceptible to enzymatic cleavage by porcine liver esterase (PLE), which can cleave off naphthol, naphthoic acid, pentanol, and hexanoic acid end groups (Figure 3a). In addition to the release of these cleaved end groups, the enzymatic cleavage should yield carboxylic acid or alcohol moieties on the dendritic block, decreasing its hydrophobicity and, thus, resulting in PEG-dendrons with a substantially higher hydrophilic/hydrophobic ratio.[63,65] The overall degradation rate of the PEG-dendrons in micellar assemblies was previously shown to depend on the equilibrium between "monomeric" PEG-dendrons and their micellar assemblies.[66] Translated to the SWCNT@PEG-dendrons, we expect their degree of enzymatic degradation to depend on the noncovalent binding interactions between the nanotubes and the hydrophobic end groups of the PEG-dendrons. Changes in the corona phase, by detaching and/or cleavage of the wrapping amphiphiles, should induce changes in the dielectric environment of the nanotubes, which can be monitored *via* their NIR-fluorescence emission.[10,27,56,67] In order to follow the PEG-dendron degradation, we incubated the SWCNT@PEG-dendrons with PLE and monitored the fluorescence response during an incubation time of 10 h. Significant fluorescence modulation could be observed for SWCNT@PEG-D-naphthyl, SWCNT@PEG-D-pentyl, and SWCNT@PEG-D-hexanoate, showing a decrease in intensity of ca. 30%, while SWCNT@PEG-D-naphthoate showed no response (Figure 3b left).

The extent of the decrease in fluorescence intensity reflects the differences in interactions between the SWCNTs and PEG-dendrons, which were mentioned above. The orientation of the ester bond in the aromatic end group significantly influenced the fluorescence response, as a result of the different electron densities of the aromatic group. However, comparing the response of the aliphatic end groups showed no significant differences between the two orientations. The absorption spectra of SWCNT@PEG-dendrons before and after incubation with PLE for 24 h showed no changes in absorption confirming that the fluorescence intensity decrease cannot be explained by simple aggregation of the SWCNTs (Figure S5, Supporting Information). Unspecific protein interaction with the SWCNT@PEG-dendrons was excluded as incubating them with bovine serum albumin (BSA), a protein commonly used for assays of nonspecific binding, showed no fluorescence response (Figure S6, Supporting Information). Monitoring the time-dependent fluorescence decrease of the (9,4) chirality for the different SWCNT@PEG-dendrons showed comparable decay rates for SWCNT@PEG-D-naphthyl, SWCNT@PEG-D-pentyl, and SWCNT@PEG-D-hexanoate and saturation after 4−5 h (Figure 3b right). Quantifying the fluorescence response of the different chiralities in each of the samples when excited at λ_{ex} = 730 nm, showed a chirality-dependent response (Figure S7 and Table S2, Supporting Information), which may

https://doi.org/10.1021/acsnano.1c09125
ACS Nano 2021, 15, 20539−20549

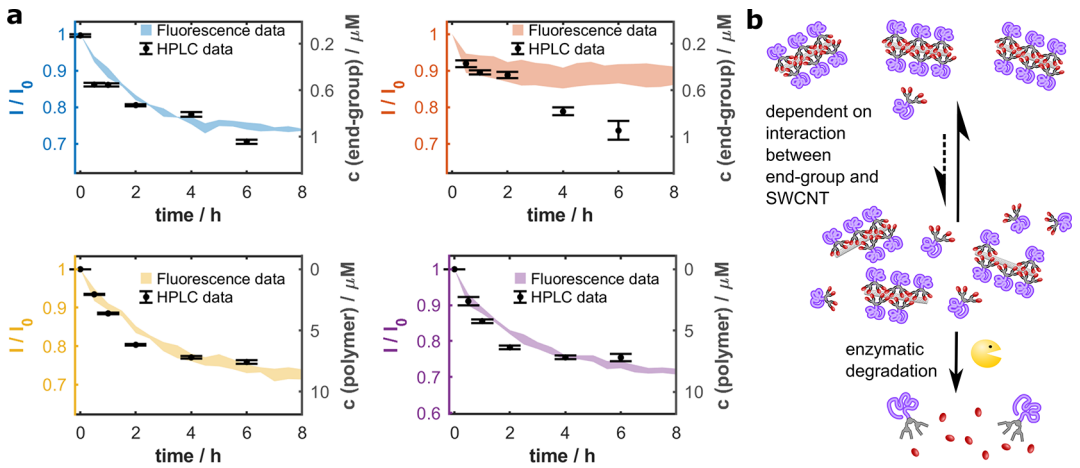

Figure 4. Correlation of the fluorescence signal with the degradation of the polymer-dendrons and proposed mechanism. (a) Correlation of the time-dependent fluorescence signal of the SWCNT@PEG-D-naphthyl (blue) with the concentration increase of the cleaved-off naphthol end group determined *via* HPLC (black; $R = -0.95$, $P = 0.003$) and of the SWCNT@PEG-D-naphthoate (red) with the concentration increase of the cleaved-off naphthoic acid end group determined *via HPLC (black; $R = -0.87$, $P = 0.022$). Correlation of the time-dependent fluorescence signal of the SWCNT@PEG-D-pentyl (yellow; $R = -0.98$, $P = 0.001$) and SWCNT@PEG-D-hexanoate (purple; $R = -0.97$, $P = 0.001$) with the generation of the cleaved polymer, measured after separation via HPLC (black). Shaded areas show mean and standard deviation. (b) Proposed equilibrium-dependent degradation mechanism, which is dependent on the interaction between SWCNT/PEG-dendron assemblies.*

be attributed to geometrical differences in available surface area or SWCNT-curvature based on previous studies.[68−72]

In order to gain a better understanding of the mechanism governing the fluorescence response to the interaction with the esterase, we used high performance liquid chromatography (HPLC) to directly follow and quantify the enzymatic degradation of the amphiphiles. To this end, SWCNT@PEG-dendrons were incubated with PLE at room temperature for 6 h in total. During the incubation, fractions of the samples were extracted for further testing. The extracted samples were mixed with acetonitrile in a 1:1 volume ratio in order to quench the enzyme activity and precipitate the SWCNT, while keeping the PEG-dendrons in solution. The same procedure was repeated for a comparable concentration of the PEG-dendrons in micellar assemblies in solution (50 $\mu g\ mL^{-1}$) without the nanotubes (Figure S8 and Table S3, Supporting Information). Taking advantage of the ability to quantify the reaction components by HPLC, we could directly follow the rate of degradation of the intact PEG-dendrons, *i.e.*, PEG-dendrons with all four end groups (Figure 3c left). In addition, owing to the spectroscopic signal of naphthol and naphthoic acid, which is lacking in the case of pentanol and hexanoic acid, we could also follow the increasing concentration of the cleaved-off end groups of PEG-D-naphthyl and PEG-D-naphthoate. In the case of PEG-D-pentanol and PEG-D-hexanoate we could monitor the generation of the cleaved polymer (Figure 3c right). For all four PEG-dendrons, the degradation process of the intact PEG-dendrons was comparable for SWCNT@PEG-dendrons and the "free" PEG-dendrons, but slightly faster for the latter. The aromatic PEG-dendrons showed a very slow and incomplete degradation process, as the samples still contained >95% of the intact PEG-dendrons after 6 h incubation time, in agreement with the concentration of the cleaved-off aromatic end groups over time. Following the degradation of the intact aliphatic PEG-dendrons as well as the generation of their cleaved PEG-dendrons without end groups, we monitor full enzymatic degradation after an incubation time of ca. 4 h. The slow degradation rate for the aromatic PEG-dendrons shows that their micellar assemblies, as well as their binding to the SWCNT surface, are much more stable. This higher stability renders them substantially less susceptible to enzymatic degradation compared to the aliphatic ones.

Relating the enzymatic degradation of the PEG-dendrons to the fluorescence response of the SWCNTs, we observe that the SWCNT@PEG-D-naphthyl shows a fluorescence signal that is consistent with its end group cleavage, while the SWCNT@PEG-D-naphthoate does not (Figure 4a), despite having a similar concentration of cleaved end groups (Figure 3c).

The significant solvatochromic shift for SWCNT@PEG-D-naphthyl upon the addition of a surfactant (Figure 2b) indicates a large surface accessibility of the SWCNT. Therefore, we expect that even minor changes in the corona phase of the SWCNTs, as evident from the fact that most of the PEG-D-naphthyl remains in its intact form (Figure 3c), can induce a strong fluorescence response, consistent with previous reports.[19] On the contrary, the PEG-D-naphthoate corona phase of the SWCNTs showed the lowest accessible surface area to surfactant perturbation (Figure 2b) and, indeed, we observe only a small fluorescence response upon PLE addition, consistent with only a minor cleavage of the PEG-D-naphthoate observed after the separation of the reaction components *via* HPLC. The results obtained after the HPLC separation cannot distinguish between PEG-dendrons that were bound directly to the SWCNT surface or PEG-dendrons that are in solution, while the fluorescence signal solely monitors events in close proximity to the SWCNT surface. Hence, we conclude that in the case of the PEG-D-naphthoate, most of the cleaved-off end groups stem from PEG-dendron molecules that are not directly bound to the SWCNTs; thus, there is no effect on the fluorescence emission of the SWCNTs.

In the case of the aliphatic PEG-dendrons, the fluorescence modulation of the SWCNT as a function of time, measured by the NIR emission of the SWCNT@PEG-dendrons, can be correlated to the generation of cleaved polymers from PEG-D-pentyl and PEG-D-hexanoate (Figure 4a). Indeed, these PEG-dendrons revealed similar initial fluorescence modulation

https://doi.org/10.1021/acsnano.1c09125
ACS Nano 2021, 15, 20539−20549

(Figure 3b), as well as similar solvatochromic shifts upon the addition of SDBS (Figure 2b), comparable to the wavelength shift of the SWCNT@PEG-D-naphthyl. It is important to note that although complete degradation of the intact aliphatic PEG-dendrons was achieved, we do not observe any aggregation of the SWCNT during the experiment, as the solution still contains all the reaction components including the cleaved end groups, the cleaved polymer, and the enzyme itself. In fact, the enzyme alone can partly stabilize SWCNTs in suspension, while hexanoic acid, one of the cleaved end groups, cannot (Figure S9).

The proposed mechanism for the enzymatic degradation of the PEG-dendrons coronae is depicted in Figure 4b. Noncovalent binding of the PEG-dendrons to the SWCNTs depends on the interactions of the respective end groups with the SWCNT surface. While aliphatic end groups undergo full degradation as was tracked by HPLC and could also be monitored *via* their fluorescence emission, the aromatic end groups led to assemblies with the SWCNTs that are much more stable but differed based on their specific $\pi-\pi$ stacking. It is important to note that as the rate of the enzymatic degradation is comparable for the case of the PEG-dendrons being free in solution or in the SWCNT@PEG-dendrons suspension (Figure 3), the effects of the specific interaction between the different end groups and the SWCNT surface is only reflected in the fluorescence response, and not in the cleavage rate. The effect of the different end groups on the fluorescence response, on the other end, can be attributed to the available surface area probed by the induced solvatochromic shift upon surfactant addition.

To demonstrate the generality of the SWCNT@PEG-dendrons as a sensing platform for enzymatic activity, we chose penicillin G amidase (PGA), an enzyme that hydrolyses penicillin G to phenylacetic acid and 6-aminopenicillanic acid.[63] Thus, we synthesized dendrons with a phenylacetamide end group as a substrate for this enzyme (PEG-D-amide, Figure 5a). Although bearing an aromatic end group, the π-electron system of the phenylacetamide group is much smaller than the ones of the naphthalene based groups. Furthermore, the carbonyl group is not conjugated to the aromatic structure and thus cannot not serve as an electron withdrawing group, which could have strengthened the interaction with the electron rich SWCNT surface, similar to the naphthoate dendron. As a result, the fluorescence modulation and the solvatochromic shift upon surfactant addition of the SWCNT@PEG-D-amide ($\Delta\lambda$ = −10.9 nm) resembles the aliphatic end groups coupled by an ester bond (Figure 5b,c), suggesting a similar expected response to enzymatic degradation. We measured the time-dependent fluorescence signal of the (9,4) chirality after the addition of PGA and compared it to the generation of cleaved polymer after the separation *via* HPLC. Indeed, similar to the aliphatic PEG-dendrons, the fluorescence signal correlates well with the generation of the cleaved polymer and thus reflects the enzymatic activity of the amidase. Comparing the amount of intact polymer before the cleavage and the cleaved polymer after 5 h incubation with the PGA confirms that the polymer was completely cleaved by the enzyme. Cleavage of PEG-D-amide in the SWCNT@ PEG-D-amide suspension and in free micellar assemblies in a comparable concentration (50 μg mL^{-1}) showed only a minute effect of the SWCNT on the cleavage rate (Figure S10, Supporting Information). These experiments show that the fluorescence modulation as well as the response of the

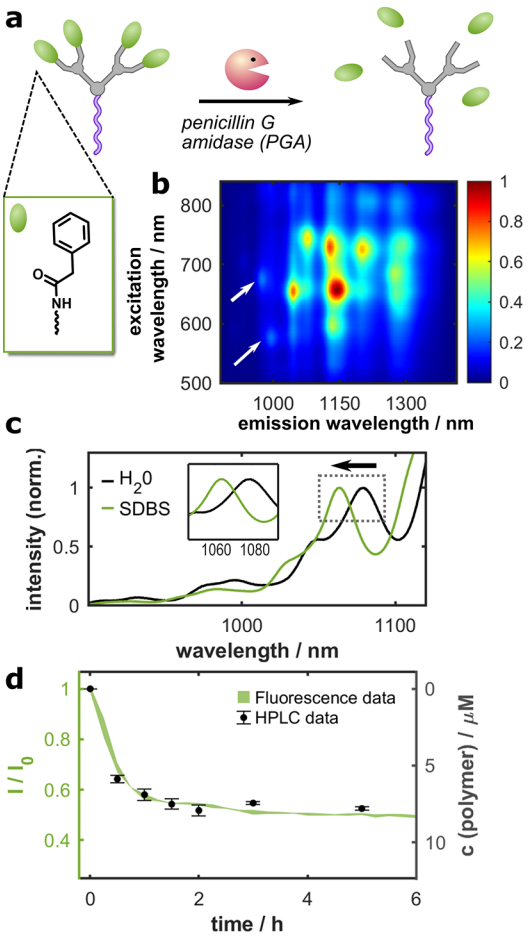

Figure 5. Measuring enzymatic activity of penicillin G amidase. (a) Cleavage of the PEG-D-amide by PGA takes place at the amide group connecting the phenylacetamide end groups to the dendron body. (b) Normalized fluorescence excitation−emission spectra for SWCNT@PEG-D-amide shows similar fluorescence emission to the aliphatic SWCNT@PEG-dendrons. (c) Wavelength shift of the (10,2) chirality upon the addition of 0.2% SDBS to a SWCNT concentration of 1 mg L^{-1}($\Delta\lambda$ = −10.9 nm). (d) Correlation of the time-dependent fluorescence signal of SWCNT@PEG-D-amide (green, shaded area shows mean and standard deviation) to the generation of the cleaved polymer (black), measured after separation *via* HPLC (R = −0.98, P < 0.001) upon addition of PGA (4.4 U mL^{-1}).

SWCNT@PEG-dendrons toward surfactant addition can already give an insight into the susceptibility of a SWCNT@ PEG-dendron assembly to enzymatic degradation.

CONCLUSIONS

We herein showed a family of amphiphilic PEG-dendrons that are able to disperse SWCNTs in water through direct interactions between their hydrophobic end groups, serving as molecular binding sites, and the graphene lattice of the SWCNTs. The two aliphatic PEG-dendrons are attached to the SWCNTs by simple hydrophobic interactions and show similar fluorescence emissions, similar accessible surface areas, and similar stabilities and reactivities toward the activating enzyme. However, due to the ester group acting either as an electron acceptor or an electron donor toward the naphthalene π-system, we observe big differences in fluorescence modulation between these end groups, including fluorescence

https://doi.org/10.1021/acsnano.1c09125
ACS Nano 2021, 15, 20539−20549

emission intensity and wavelength. Using enzymatic degradation of the PEG-dendrons by esterase as a model, we show that we can translate the enzymatic cleavage of the end groups into a spectral response of the SWCNTs. Interestingly, the accessible surface area can be correlated with the ability of the SWCNT@PEG-dendrons to show spectral responses toward the activating enzyme. Building on these findings, we were able to further design PEG-dendron amphiphiles whose end groups contain an amide bond that can suspend SWCNT, and utilize it to successfully monitor amidase activity on the SWCNT@PEG-dendron complexes through the fluorescence signal. In essence, we identified the criteria of the SWCNT sensors (fluorescence modulation and surface accessibility) needed in order to report the enzymatic cleavage of the end groups.

The amphiphilic polymer-dendron hybrids introduced here are tailorable macromolecules synthesized with high molecular precision and overall yields (ca. 90%), whose structures and compositions can be easily tuned simply by changing the hydrophobic end groups, branching unit, and hydrophilic polymer. We demonstrate here that these versatile polymer-dendron structures can be used for designing modular enzyme-responsive NIR-fluorescent SWCNT as the dendron can be tailored to have branches with varying flexibility and generation number, resulting in different numbers of end groups and interaction sites on the SWCNT surface. Furthermore, the polymer chain can vary in charge, flexibility, and conductivity or can even be designed to attach additional recognition elements or functional groups. This platform of configurable functional composite nanomaterials offers the opportunity to tailor it for not only numerous applications studying stability, reactivity, and susceptibility to enzymatic activity but also analyte binding in real-time through the transient modulation of the fluorescence emission in the NIR. Optical sensors emitting light in the NIR can be more easily implemented in *in vivo* studies, which broadens the possibilities for future applications.

EXPERIMENTAL SECTION

Synthesis of PEG-Dendron Amphiphiles. The PEG-dendron amphiphiles were synthesized in a two-step synthesis starting from monomethoxy 5 kDa polyethylene glycol diamine ($mPEG_{5kDa}$-$(NH_2)_2$. The two terminal amines were reacted with bis-allyl functionalized AB_2 branching units forming stable amide bonds. In the second step the designated cleavable hydrophobic end groups were coupled to the polymer using the photoinitiated thiol−ene click reaction. All amphiphiles were obtained in high yields and were characterized using ^{1}H NMR, GPC, and MALDI-TOF. For additional synthetic information and spectroscopic data please see the Supporting Information.

Suspension of SWCNTs with Sodium Cholate. To suspend the SWCNTs with sodium cholate, 10 mg of HiPCO SWCNTs in 20 mL of 2% (w/v) sodium cholate were bath sonicated for 10 min and subsequently tip sonicated for 2× 30 min on ice (12 W). To remove nanotube bundles and impurities, the resulting suspension was ultracentrifuged for 4 h at 40,000*g* (Optima XPN-80 ultracentrifuge, Beckman Coulter). The concentration of SWCNT@SC was determined spectroscopically (c(SWCNT@SC) = 220 mg L^{-1}) with an extinction coefficient of ε_{632nm} = 0.036 L · mg $^{-1}$ · cm $^{-1}$.

Surfactant exchange of SWCNTs with PEG-dendrons. Surfactant exchange was performed *via* dialysis from SWCNT@SC as described previously.[27] Briefly, a suspension of SWCNT@SC (40 mg L^{-1}) in 2% (w/v) sodium cholate and the respective PEG-dendron (2 mg/mL) in a total volume of 7 mL were dialyzed (GeBAflex Mega, 3.5 kDa MWCO) against water for 5 days, with daily water exchange. After the dialysis, SWCNT@PEG-dendrons were centrifuged for 30 min at 20,000*g* to remove aggregates. The supernatant suspension was washed 3 times with PBS buffer (pH 7.4) in an Amicon centrifugal filter (100 kDa MWCO, 25 min, 4,400*g*). The concentration of SWCNT@PEG-Dendron suspensions was determined as described above.[27]

Absorption Spectroscopy. Absorption spectra were recorded in a UV−vis−NIR spectrophotometer (Shimadzu UV-3600 Plus) in a wavelength range of 200−1400 nm.

NIR-Fluorescence Spectroscopy of Carbon Nanotubes. Fluorescence emission spectra were recorded in a 96-well plate mounted on an inverted microscope (Olympus IX73). A supercontinuum white-light laser (NKT-photonics, Super-K Extreme) with a bandwidth filter (NKT-photonics, Super-K varia, $\Delta\lambda$ = 20 nm) was coupled into the microscope as the excitation source. If not stated otherwise, spectra were recorded at an excitation wavelength of λ_{ex} = 730 nm with 8.5 mW. Fluorescence emission was spectrally resolved using a spectrograph (Spectra Pro HRS-300, Princeton Instruments) with a slit-width of 500 μm and a grating (150 g/mm). The fluorescence intensity spectrum was recorded by an InGaAs-camera (PylonIR, Teledyne Princeton Instruments) with 1 s exposure time for c(SWCNT) = 5 mg L^{-1} or 5 s for c(SWCNT) = 1 mg L^{-1}. Excitation−emission maps were recorded using an excitation wavelength range of 500 to 840 nm in 2 nm steps.

Enzymatic Degradation of PEG-Dendrons Wrapping around SWCNTs. Aliquots of 147 μL of SWCNT@PEG-dendrons in PBS (1 mg L^{-1} SWCNT) were placed in a 96-well plate, and treated with 3 μL of PLE to a final enzyme concentration of 1.5 μM or 3 μL of PBS as a control for 10 h incubation time. Fluorescence emission of the samples was measured in time intervals of 30 min at an excitation wavelength of λ_{ex} = 730 nm. Experiments with SWCNT@PEG-D-amide and PGA were conducted accordingly with a final PGA concentration of 4.4 U mL^{-1}.

Separation and Quantification of the Reaction Components of the Degradation Process *via* HPLC. HPLC measurements were recorded on a Waters Alliance e2695 separations module equipped with a Waters 2998 photodiode array detector. A total volume of 10 mL containing SWCNT@PEG-dendrons (c(SWCNT) = 1 mg L^{-1}) and PLE (1.5 μM) or PGA (4.4 U mL^{-1}) and a control containing only PEG-dendrons (50 μg mL^{-1}) and PLE (1.5 μM) or PGA (4.4 U mL^{-1}) were incubated. At time intervals of 0 h, 30 min, 1 h, 2 h, 4 h, and 6 h (0 h, 30 min, 1 h, 1.5 h, 2 h, 3 h, and 5 h, for PGA), a volume of 1 mL was taken from the samples and subjected to 1 mL of acetonitrile to precipitate the SWCNTs while keeping the PEG-dendrons and the cleavage products in suspension. The solution was filtered with a 0.2 μm PTFE syringe filter to remove SWCNTs. A total of 60 μL of the samples was injected into HPLC. For the quantification of the reaction components, we integrated the peaks assigned to the intact polymer-dendrons (bearing all 4 end groups) at absorption wavelengths of λ = 225 nm (PEG-D-naphthyl), λ = 236 nm (PEG-D-naphthoate), and λ = 297 nm (PEG-D-pentyl and PEG-D-hexanoate). In the case of PEG-D-naphthyl and PEG-D-naphthoate we integrated the peaks assigned to the cleaved-off end groups, naphthol and naphthoic acid, at absorption wavelengths of λ = 225 nm and λ = 236 nm, respectively. The concentrations of the cleaved-off end groups were determined *via* a calibration curve, determined by the area of the peak for naphthol (λ = 225 nm) and naphthoic acid (λ = 236 nm) at concentrations of 1, 5, and 10 μM. In the case of PEG-D-pentyl, PEG-D-hexanoate, and PEG-D-amide we integrated the peaks assigned to the cleaved polymer at an absorption wavelength of λ = 297 nm.

ASSOCIATED CONTENT

Supporting Information

The Supporting Information is available free of charge at https://pubs.acs.org/doi/10.1021/acsnano.1c09125.

Detailed materials and method section, detailed synthesis and characterization of PEG-dendrons, images showing surfactant exchange with PEG-D-COOH,

https://doi.org/10.1021/acsnano.1c09125
ACS Nano 2021, 15, 20539−20549

absorption and fluorescence spectra of all SWCNT@PEG-dendrons, comparison between absorption and fluorescence spectra of all SWCNT@PEG-dendrons, absorption spectra before and after cleavage, fluorescence response of SWCNT@PEG-dendrons to BSA, fluorescence response and decay rates of the different chiralities, UV-absorption spectra of SWCNT@PEG-dendrons and free PEG-dendrons, generation of cleaved polymer for SWCNT@PEG-D-amide and free PEG-D-amide (PDF)

AUTHOR INFORMATION

Corresponding Authors

Roey J. Amir − *Department of Organic Chemistry, School of Chemistry, Faculty of Exact Sciences, Tel-Aviv University, Tel-Aviv 6997801, Israel; The Center for Physics and Chemistry of Living Systems, Center for Nanoscience and Nanotechnology, and ADAMA Center for Novel Delivery Systems in Crop Protection, Tel-Aviv University, Tel Aviv 6997801, Israel;* orcid.org/0000-0002-8502-3302; Email: amirroey@tauex.tau.ac.il

Gili Bisker − *Department of Biomedical Engineering, Faculty of Engineering, Tel-Aviv University, Tel Aviv 6997801, Israel; The Center for Physics and Chemistry of Living Systems, Center for Nanoscience and Nanotechnology, and Center for Light Matter Interaction, Tel-Aviv University, Tel Aviv 6997801, Israel;* orcid.org/0000-0003-2592-7956; Email: bisker@tauex.tau.ac.il

Authors

Verena Wulf − *Department of Biomedical Engineering, Faculty of Engineering, Tel-Aviv University, Tel Aviv 6997801, Israel;* orcid.org/0000-0003-0155-9829

Gadi Slor − *Department of Organic Chemistry, School of Chemistry, Faculty of Exact Sciences, Tel-Aviv University, Tel-Aviv 6997801, Israel; The Center for Physics and Chemistry of Living Systems and Center for Nanoscience and Nanotechnology, Tel-Aviv University, Tel Aviv 6997801, Israel;* orcid.org/0000-0002-5379-6407

Parul Rathee − *Department of Organic Chemistry, School of Chemistry, Faculty of Exact Sciences, Tel-Aviv University, Tel-Aviv 6997801, Israel; The Center for Physics and Chemistry of Living Systems and Center for Nanoscience and Nanotechnology, Tel-Aviv University, Tel Aviv 6997801, Israel*

Complete contact information is available at: https://pubs.acs.org/10.1021/acsnano.1c09125

Author Contributions

The manuscript was written through contributions of all authors. All authors have given approval to the final version of the manuscript.

Notes

The authors declare no competing financial interest.

A preprint of this paper was published previously on chemrxiv.org: Wulf, V.; Slor, G.; Rathee, P.; Amir, R. J.; Bisker, G.; Dendron−Polymer Hybrids as Tailorable Coronae of Single-Walled Carbon Nanotubes. 2021, ChemRxiv. https://chemrxiv.org/engage/chemrxiv/article-details/60c757b7f96a004a8f288d04 (accessed November 25, 2021).

[▽]V.W., G.S., and P.R. contributed equally.

ACKNOWLEDGMENTS

G. Bisker acknowledges the support of the Zuckerman STEM Leadership Program, the Israel Science Foundation (grant No. 456/18), the Ministry of Science, Technology, and Space, Israel (grant No. 3-17426), the Tel Aviv University Center for Combatting Pandemics, the Zimin Institute for Engineering Solutions Advancing Better Lives, and the Nicholas and Elizabeth Slezak Super Center for Cardiac Research and Biomedical Engineering at Tel Aviv University. R. J. Amir thanks the Israel Science Foundation (grant No. 1553/18) for the support of this research. G. Slor thanks the Marian Gertner Institute for Medical Nanosystems in Tel Aviv University for their financial support.

REFERENCES

(1) Jain, A.; Homayoun, A.; Bannister, C. W.; Yum, K. Single-Walled Carbon Nanotubes as Near-Infrared Optical Biosensors for Life Sciences and Biomedicine. *Biotechnol. J.* **2015**, *10*, 447−459.

(2) Mann, F. A.; Lv, Z.; Großhans, J.; Opazo, F.; Kruss, S. Nanobody-Conjugated Nanotubes for Targeted Near-Infrared *in Vivo* Imaging and Sensing. *Angew. Chem., Int. Ed.* **2019**, *58*, 11469−11473.

(3) Welsher, K.; Sherlock, S. P.; Dai, H. Deep-Tissue Anatomical Imaging of Mice Using Carbon Nanotube Fluorophores in the Second Near-Infrared Window. *Proc. Natl. Acad. Sci. U. S. A.* **2011**, *108*, 8943−8948.

(4) Iverson, N. M.; Bisker, G.; Farias, E.; Ivanov, V.; Ahn, J.; Wogan, G. N.; Strano, M. S. Quantitative Tissue Spectroscopy of Near Infrared Fluorescent Nanosensor Implants. *J. Biomed. Nanotechnol.* **2016**, *12*, 1035−1047.

(5) Godin, A. G.; Varela, J. A.; Gao, Z.; Danné, N.; Dupuis, J. P.; Lounis, B.; Groc, L.; Cognet, L. Single-Nanotube Tracking Reveals the Nanoscale Organization of the Extracellular Space in the Live Brain. *Nat. Nanotechnol.* **2017**, *12*, 238−243.

(6) Beyene, A. G.; Delevich, K.; Del Bonis-O'Donnell, J. T.; Piekarski, D. J.; Lin, W. C.; Thomas, A. W.; Yang, S. J.; Kosillo, P.; Yang, D.; Prounis, G. S.; Wilbrecht, L.; Landry, M. P. Imaging Striatal Dopamine Release Using a Nongenetically Encoded Infrared Fluorescent Catecholamine Nanosensor. *Sci. Adv.* **2019**, *5*, No. eaaw3108.

(7) Hofferber, E. M.; Stapleton, J. A.; Iverson, N. M. Single Walled Carbon Nanotubes as Optical Sensors for Biological Applications. *J. Electrochem. Soc.* **2020**, *167*, 037530.

(8) Saito, R.; Grüneis, A.; Samsonidze, G. G.; Dresselhaus, G.; Dresselhaus, M. S.; Jorio, A.; Cançado, L. G.; Pimenta, M. A.; Souza Filho, A. G. Optical Absorption of Graphite and Single-Wall Carbon Nanotubes. *Appl. Phys. A: Mater. Sci. Process.* **2004**, *78*, 1099−1105.

(9) Bachilo, S. M.; Strano, M. S.; Kittrell, C.; Hauge, R. H.; Smalley, R. E.; Weisman, R. B. Structure-Assigned Optical Spectra of Single-Walled Carbon Nanotubes. *Science* **2002**, *298*, 2361−2366.

(10) Gao, J.; Gomulya, W.; Loi, M. A. Effect of Medium Dielectric Constant on the Physical Properties of Single-Walled Carbon Nanotubes. *Chem. Phys.* **2013**, *413*, 35−38.

(11) Campo, J.; Cambré, S.; Botka, B.; Obrzut, J.; Wenseleers, W.; Fagan, J. A. Optical Property Tuning of Single-Wall Carbon Nanotubes by Endohedral Encapsulation of a Wide Variety of Dielectric Molecules. *ACS Nano* **2021**, *15*, 2301−2317.

(12) Jain, R. M.; Ben-Naim, M.; Landry, M. P.; Strano, M. S. Competitive Binding in Mixed Surfactant Systems for Single-Walled Carbon Nanotube Separation. *J. Phys. Chem. C* **2015**, *119*, 22737−22745.

(13) Zheng, M.; Jagota, A.; Semke, E. D.; Diner, B. A.; McLean, R. S.; Lustig, S. R.; Richardson, R. E.; Tassi, N. G. DNA-Assisted Dispersion and Separation of Carbon Nanotubes. *Nat. Mater.* **2003**, *2*, 338−342.

(14) Landry, M. P.; Vuković, L.; Kruss, S.; Bisker, G.; Landry, A. M.; Islam, S.; Jain, R.; Schulten, K.; Strano, M. S. Comparative Dynamics and Sequence Dependence of DNA and RNA Binding to Single

Walled Carbon Nanotubes. *J. Phys. Chem. C* **2015**, *119*, 10048−10058.
(15) Antonucci, A.; Kupis-Rozmysłowicz, J.; Boghossian, A. A. Noncovalent Protein and Peptide Functionalization of Single-Walled Carbon Nanotubes for Biodelivery and Optical Sensing Applications. *ACS Appl. Mater. Interfaces* **2017**, *9*, 11321−11331.
(16) Oliveira, S. F.; Bisker, G.; Bakh, N. A.; Gibbs, S. L.; Landry, M. P.; Strano, M. S. Protein Functionalized Carbon Nanomaterials for Biomedical Applications. *Carbon* **2015**, *95*, 767−779.
(17) Mann, F. A.; Horlebein, J.; Meyer, N. F.; Meyer, D.; Thomas, F.; Kruss, S. Carbon Nanotubes Encapsulated in Coiled-Coil Peptide Barrels. *Chem. - Eur. J.* **2018**, *24*, 12241−12245.
(18) Shumeiko, V.; Paltiel, Y.; Bisker, G.; Hayouka, Z.; Shoseyov, O. A Paper-Based Near-Infrared Optical Biosensor for Quantitative Detection of Protease Activity Using Peptide-Encapsulated SWCNTs. *Sensors* **2020**, *20*, 5247.
(19) Chio, L.; Del Bonis-O'Donnell, J. T.; Kline, M. A.; Kim, J. H.; McFarlane, I. R.; Zuckermann, R. N.; Landry, M. P. Electrostatic Assemblies of Single-Walled Carbon Nanotubes and Sequence-Tunable Peptoid Polymers Detect a Lectin Protein and Its Target Sugars. *Nano Lett.* **2019**, *19*, 7563−7572.
(20) Fernandes, R. M. F.; Dai, J.; Regev, O.; Marques, E. F.; Furó, I. Block Copolymers as Dispersants for Single-Walled Carbon Nanotubes: Modes of Surface Attachment and Role of Block Polydispersity. *Langmuir* **2018**, *34*, 13672−13679.
(21) Budhathoki-Uprety, J.; Harvey, J. D.; Isaac, E.; Williams, R. M.; Galassi, T. V.; Langenbacher, R. E.; Heller, D. A. Polymer Cloaking Modulates the Carbon Nanotube Protein Corona and Delivery into Cancer Cells. *J. Mater. Chem. B* **2017**, *5*, 6637−6644.
(22) Harvey, J. D.; Jena, P. V.; Baker, H. A.; Zerze, G. H.; Williams, R. M.; Galassi, T. V.; Roxbury, D.; Mittal, J.; Heller, D. A. A Carbon Nanotube Reporter of MicroRNA Hybridization Events *in Vivo*. *Nat. Biomed. Eng.* **2017**, *1*, 0041.
(23) Landry, M. P.; Ando, H.; Chen, A. Y.; Cao, J.; Kottadiel, V. I.; Chio, L.; Yang, D.; Dong, J.; Lu, T. K.; Strano, M. S. Single-Molecule Detection of Protein Efflux from Microorganisms Using Fluorescent Single-Walled Carbon Nanotube Sensor Arrays. *Nat. Nanotechnol.* **2017**, *12*, 368−377.
(24) So, H. M.; Won, K.; Kim, Y. H.; Kim, B. K.; Ryu, B. H.; Na, P. S.; Kim, H.; Lee, J. O. Single-Walled Carbon Nanotube Biosensors Using Aptamers as Molecular Recognition Elements. *J. Am. Chem. Soc.* **2005**, *127*, 11906−11907.
(25) Zhang, J.; Landry, M. P.; Barone, P. W.; Kim, J.-H.; Lin, S.; Ulissi, Z. W.; Lin, D.; Mu, B.; Boghossian, A. A.; Hilmer, A. J.; Rwei, A.; Hinckley, A. C.; Kruss, S.; Shandell, M. A.; Nair, N.; Blake, S.; Şen, F.; Şen, S.; Croy, R. G.; Li, D.; Yum, K.; Ahn, J.-H.; Jin, H.; Heller, D. A.; Essigmann, J. M.; Blankschtein, D.; Strano, M. S. Molecular Recognition Using Corona Phase Complexes Made of Synthetic Polymers Adsorbed on Carbon Nanotubes. *Nat. Nanotechnol.* **2013**, *8*, 959−968.
(26) Kruss, S.; Landry, M. P.; Vander Ende, E.; Lima, B. M. A.; Reuel, N. F.; Zhang, J.; Nelson, J.; Mu, B.; Hilmer, A.; Strano, M. Neurotransmitter Detection Using Corona Phase Molecular Recognition on Fluorescent Single-Walled Carbon Nanotube Sensors. *J. Am. Chem. Soc.* **2014**, *136*, 713−724.
(27) Bisker, G.; Dong, J.; Park, H. D.; Iverson, N. M.; Ahn, J.; Nelson, J. T.; Landry, M. P.; Kruss, S.; Strano, M. S. Protein-Targeted Corona Phase Molecular Recognition. *Nat. Commun.* **2016**, *7*, 10241.
(28) Hendler-Neumark, A.; Bisker, G. Fluorescent Single-Walled Carbon Nanotubes for Protein Detection. *Sensors* **2019**, *19*, 5403.
(29) Amir, D.; Hendler-Neumark, A.; Wulf, V.; Ehrlich, R.; Bisker, G. Oncometabolite Fingerprinting Using Fluorescent Single-Walled Carbon Nanotubes *Adv. Mater. Interfaces*, in press.
(30) Bisker, G.; Bakh, N. A.; Lee, M. A.; Ahn, J.; Park, M.; O'Connell, E. B.; Iverson, N. M.; Strano, M. S. Insulin Detection Using a Corona Phase Molecular Recognition Site on Single-Walled Carbon Nanotubes. *ACS Sensors* **2018**, *3*, 367−377.
(31) Ehrlich, R.; Hendler-Neumark, A.; Wulf, V.; Amir, D.; Bisker, G. Optical Nanosensors for Real-Time Feedback on Insulin Secretion by β-Cells. *Small* **2021**, *17*, 2101660.
(32) Pinals, R. L.; Ledesma, F.; Yang, D.; Navarro, N.; Jeong, S.; Pak, J. E.; Kuo, L.; Chuang, Y. C.; Cheng, Y. W.; Sun, H. Y.; Landry, M. P. Rapid SARS-CoV-2 Spike Protein Detection by Carbon Nanotube-Based Near-Infrared Nanosensors. *Nano Lett.* **2021**, *21*, 2272−2280.
(33) Cho, S.-Y.; Jin, X.; Gong, X.; Yang, S.; Cui, J.; Strano, M. S. Antibody-Free Rapid Detection of SARS-CoV-2 Proteins Using Corona Phase Molecular Recognition to Accelerate Development Time. *Anal. Chem.* **2021**, *93*, 14685−14693.
(34) Zvi, Y.; Yoona, Y.; Elana, A.; Christian, C.; H, S. A.; Quinlan, C.; Winson, C.; Long, R. K.; A, L. D.; Martin, F.; Lakshmi, R.; Ming, Z.; Anand, J.; A, H. D. A Perception-Based Nanosensor Platform to Detect Cancer Biomarkers. *Sci. Adv.* **2021**, *7*, No. eabj0852.
(35) Gillen, A. J.; Boghossian, A. A. Non-Covalent Methods of Engineering Optical Sensors Based on Single-Walled Carbon Nanotubes. *Front. Chem.* **2019**, *7*, 612.
(36) Lambert, B.; Gillen, A. J.; Schuergers, N.; Wu, S.-J.; Boghossian, A. A. Directed Evolution of the Optoelectronic Properties of Synthetic Nanomaterials. *Chem. Commun.* **2019**, *55*, 3239−3242.
(37) Jeong, S.; Yang, D.; Beyene, A. G.; Del Bonis-O'Donnell, J. T.; Gest, A. M. M.; Navarro, N.; Sun, X.; Landry, M. P. High-Throughput Evolution of Near-Infrared Serotonin Nanosensors. *Sci. Adv.* **2019**, *5*, No. eaay3771.
(38) Dong, J.; Lee, M. A.; Rajan, A. G.; Rahaman, I.; Sun, J. H.; Park, M.; Salem, D. P.; Strano, M. S. A Synthetic Mimic of Phosphodiesterase Type 5 Based on Corona Phase Molecular Recognition of Single-Walled Carbon Nanotubes. *Proc. Natl. Acad. Sci. U. S. A.* **2020**, *117*, 26616−26625.
(39) Lee, M. A.; Wang, S.; Jin, X.; Bakh, N. A.; Nguyen, F. T.; Dong, J.; Silmore, K. S.; Gong, X.; Pham, C.; Jones, K. K.; Muthupalani, S.; Bisker, G.; Son, M.; Strano, M. S. Implantable Nanosensors for Human Steroid Hormone Sensing *in Vivo* Using a Self-Templating Corona Phase Molecular Recognition. *Adv. Healthcare Mater.* **2020**, *9*, 2000429.
(40) Shumeiko, V.; Malach, E.; Helman, Y.; Paltiel, Y.; Bisker, G.; Hayouka, Z.; Shoseyov, O. A Nanoscale Optical Biosensor Based on Peptide Encapsulated SWCNTs for Detection of Acetic Acid in the Gaseous Phase. *Sens. Actuators, B* **2021**, *327*, 128832.
(41) Shumeiko, V.; Paltiel, Y.; Bisker, G.; Hayouka, Z.; Shoseyov, O. A Nanoscale Paper-Based Near-Infrared Optical Nose (NIRON). *Biosens. Bioelectron.* **2021**, *172*, 112763.
(42) Gitsov, I.; Wooley, K. L.; Fréchet, J. M. J. Novel Polyether Copolymers Consisting of Linear and Dendritic Blocks. *Angew. Chem., Int. Ed. Engl.* **1992**, *31*, 1200−1202.
(43) Gitsov, I.; Wooley, K. L.; Hawker, C. J.; Ivanova, P. T.; Fréchet, J. M. J. Synthesis and Properties of Novel Linear-Dendritic Block Copolymers. Reactivity of Dendritic Macromolecules toward Linear Polymers. *Macromolecules* **1993**, *26*, 5621−5627.
(44) Whitton, G.; Gillies, E. R. Functional Aqueous Assemblies of Linear-Dendron Hybrids. *J. Polym. Sci., Part A: Polym. Chem.* **2015**, *53*, 148−172.
(45) Gitsov, I. Hybrid Linear Dendritic Macromolecules: From Synthesis to Applications. *J. Polym. Sci., Part A: Polym. Chem.* **2008**, *46*, 5295−5314.
(46) Slor, G.; Olea, A. R.; Pujals, S.; Tigrine, A.; De La Rosa, V. R.; Hoogenboom, R.; Albertazzi, L.; Amir, R. J. Judging Enzyme-Responsive Micelles by Their Covers: Direct Comparison of Dendritic Amphiphiles with Different Hydrophilic Blocks. *Biomacromolecules* **2021**, *22*, 1197−1210.
(47) Bahun, G. J.; Adronov, A. Interactions of Carbon Nanotubes with Pyrene-Functionalized Linear-Dendritic Hybrid Polymers. *J. Polym. Sci., Part A: Polym. Chem.* **2010**, *48*, 1016−1028.
(48) Setaro, A.; Popeney, C. S.; Trappmann, B.; Datsyuk, V.; Haag, R.; Reich, S. Polyglycerol-Derived Amphiphiles for Single Walled Carbon Nanotube Suspension. *Chem. Phys. Lett.* **2010**, *493*, 147−150.

https://doi.org/10.1021/acsnano.1c09125
ACS Nano 2021, 15, 20539−20549

(49) Ernst, F.; Heek, T.; Setaro, A.; Haag, R.; Reich, S. Functional Surfactants for Carbon Nanotubes: Effects of Design. *J. Phys. Chem. C* **2013**, *117*, 1157−1162.
(50) Ernst, F.; Gao, Z.; Arenal, R.; Heek, T.; Setaro, A.; Fernandez-Pacheco, R.; Haag, R.; Cognet, L.; Reich, S. Noncovalent Stable Functionalization Makes Carbon Nanotubes Hydrophilic and Biocompatible. *J. Phys. Chem. C* **2017**, *121*, 18887−18891.
(51) Gutierrez-Ulloa, C. E.; Buyanova, M. Y.; Apartsin, E. K.; Venyaminova, A. G.; de la Mata, F. J.; Gómez, R. Carbon Nanotubes Decorated with Cationic Carbosilane Dendrons and Their Hybrids with Nucleic Acids. *ChemNanoMat* **2018**, *4*, 220−230.
(52) Maeda, Y.; Konno, Y.; Yamada, M.; Zhao, P.; Zhao, X.; Ehara, M.; Nagase, S. Control of Near Infrared Photoluminescence Properties of Single-Walled Carbon Nanotubes by Functionalization with Dendrons. *Nanoscale* **2018**, *10*, 23012−23017.
(53) Iverson, N. M.; Barone, P. W.; Shandell, M.; Trudel, L. J.; Sen, S.; Sen, F.; Ivanov, V.; Atolia, E.; Farias, E.; McNicholas, T. P.; Reuel, N.; Parry, N. M. A.; Wogan, G. N.; Strano, M. S. *In Vivo* Biosensing *via* Tissue-Localizable Near-Infrared-Fluorescent Single-Walled Carbon Nanotubes. *Nat. Nanotechnol.* **2013**, *8*, 873−880.
(54) Poenitzsch, V. Z.; Winters, D. C.; Xie, H.; Dieckmann, G. R.; Dalton, A. B.; Musselman, I. H. Effect of Electron-Donating and Electron-Withdrawing Groups on Peptide/Single-Walled Carbon Nanotube Interactions. *J. Am. Chem. Soc.* **2007**, *129*, 14724−14732.
(55) Welsher, K.; Liu, Z.; Sherlock, S. P.; Robinson, J. T.; Chen, Z.; Daranciang, D.; Dai, H. A Route to Brightly Fluorescent Carbon Nanotubes for Near-Infrared Imaging in Mice. *Nat. Nanotechnol.* **2009**, *4*, 773−780.
(56) Hertel, T.; Hagen, A.; Talalaev, V.; Arnold, K.; Hennrich, F.; Kappes, M.; Rosenthal, S.; McBride, J.; Ulbricht, H.; Flahaut, E. Spectroscopy of Single- and Double-Wall Carbon Nanotubes in Different Environments. *Nano Lett.* **2005**, *5*, 511−514.
(57) Kuang, Z.; Berger, F. J.; Lustres, J. L. P.; Wollscheid, N.; Li, H.; Lüttgens, J.; Leinen, M. B.; Flavel, B. S.; Zaumseil, J.; Buckup, T. Charge Transfer from Photoexcited Semiconducting Single-Walled Carbon Nanotubes to Wide-Bandgap Wrapping Polymer. *J. Phys. Chem. C* **2021**, *125*, 8125−8136.
(58) Papadopoulos, I.; Menon, A.; Plass, F.; Molina, D.; Harreiß, C.; Kahnt, A.; Spiecker, E.; Sastre-Santos, Á.; Guldi, D. M. Efficient Charge-Transfer from Diketopyrrolopyrroles to Single-Walled Carbon Nanotubes. *Nanoscale* **2021**, *13*, 11544−11551.
(59) Park, M.; Salem, D. P.; Parviz, D.; Gong, X.; Silmore, K. S.; Lew, T. T. S.; Khong, D. T.; Ang, M. C.-Y.; Kwak, S.-Y.; Chan-Park, M. B.; Strano, M. S. Measuring the Accessible Surface Area within the Nanoparticle Corona Using Molecular Probe Adsorption. *Nano Lett.* **2019**, *19*, 7712−7724.
(60) Zheng, Y.; Alizadehmojarad, A. A.; Bachilo, S. M.; Kolomeisky, A. B.; Weisman, R. B. Dye Quenching of Carbon Nanotube Fluorescence Reveals Structure-Selective Coating Coverage. *ACS Nano* **2020**, *14*, 12148−12158.
(61) Roxbury, D.; Tu, X.; Zheng, M.; Jagota, A. Recognition Ability of DNA for Carbon Nanotubes Correlates with Their Binding Affinity. *Langmuir* **2011**, *27*, 8282−8293.
(62) Harnoy, A. J.; Buzhor, M.; Tirosh, E.; Shaharabani, R.; Beck, R.; Amir, R. J. Modular Synthetic Approach for Adjusting the Disassembly Rates of Enzyme-Responsive Polymeric Micelles. *Biomacromolecules* **2017**, *18*, 1218−1228.
(63) Slor, G.; Papo, N.; Hananel, U.; Amir, R. J. Tuning the Molecular Weight of Polymeric Amphiphiles as a Tool to Access Micelles with a Wide Range of Enzymatic Degradation Rates. *Chem. Commun.* **2018**, *54*, 6875−6878.
(64) Segal, M.; Avinery, R.; Buzhor, M.; Shaharabani, R.; Harnoy, A. J.; Tirosh, E.; Beck, R.; Amir, R. J. Molecular Precision and Enzymatic Degradation: From Readily to Undegradable Polymeric Micelles by Minor Structural Changes. *J. Am. Chem. Soc.* **2017**, *139*, 803−810.
(65) Harnoy, A. J.; Rosenbaum, I.; Tirosh, E.; Ebenstein, Y.; Shaharabani, R.; Beck, R.; Amir, R. J. Enzyme-Responsive Amphiphilic PEG-Dendron Hybrids and Their Assembly into Smart Micellar Nanocarriers. *J. Am. Chem. Soc.* **2014**, *136*, 7531−7534.
(66) Slor, G.; Amir, R. J. Using High Molecular Precision to Study Enzymatically Induced Disassembly of Polymeric Nanocarriers: Direct Enzymatic Activation or Equilibrium-Based Degradation? *Macromolecules* **2021**, *54*, 1577−1588.
(67) Heller, D. A.; Pratt, G. W.; Zhang, J.; Nair, N.; Hansborough, A. J.; Boghossian, A. A.; Reuel, N. F.; Barone, P. W.; Strano, M. S. Peptide Secondary Structure Modulates Single-Walled Carbon Nanotube Fluorescence as a Chaperone Sensor for Nitroaromatics. *Proc. Natl. Acad. Sci. U. S. A.* **2011**, *108*, 8544−8549.
(68) Wu, Q. Y.; Tian, W. De; Ma, Y. Q. Nanopatterns of Phospholipid Assemblies on Carbon Nanotubes: A Molecular Dynamics Simulation Study. *J. Phys. Chem. C* **2018**, *122*, 7455−7463.
(69) Yurekli, K.; Mitchell, C. A.; Krishnamoorti, R. Small-Angle Neutron Scattering from Surfactant-Assisted Aqueous Dispersions of Carbon Nanotubes. *J. Am. Chem. Soc.* **2004**, *126*, 9902−9903.
(70) Salem, D. P.; Landry, M. P.; Bisker, G.; Ahn, J.; Kruss, S.; Strano, M. S. Chirality Dependent Corona Phase Molecular Recognition of DNA-Wrapped Carbon Nanotubes. *Carbon* **2016**, *97*, 147−153.
(71) Fagan, J. A. Aqueous Two-Polymer Phase Extraction of Single-Wall Carbon Nanotubes Using Surfactants. *Nanoscale Adv.* **2019**, *1*, 3307−3324.
(72) Zheng, M. Sorting Carbon Nanotubes. *Single-Walled Carbon Nanotubes. Topics in Current Chemistry Collections*; Springer: Cham, 2019; pp 129−164.

https://doi.org/10.1021/acsnano.1c09125
ACS Nano 2021, 15, 20539−20549